1,4-Benzoquinone antimicrobial agents against *Staphylococcus aureus* and *Mycobacterium tuberculosis* derived from scorpion venom

Edson Norberto Carcamo-Noriega[a,1], Shyam Sathyamoorthi[b,1], Shibdas Banerjee[b,c,1], Elumalai Gnanamani[b], Monserrat Mendoza-Trujillo[d], Dulce Mata-Espinosa[d], Rogelio Hernández-Pando[d], José Ignacio Veytia-Bucheli[a], Lourival D. Possani[a,2], and Richard N. Zare[b,2]

[a]Department of Molecular Medicine and Bioprocesses, Instituto de Biotecnologia, Universidad Nacional Autonoma de Mexico, 62210 Morelos, Mexico; [b]Department of Chemistry, Stanford University, Stanford, CA 94305; [c]Department of Chemistry, Indian Institute of Science Education and Research Tirupati, Tirupati 517507, India; and [d]Section of Experimental Pathology, Department of Pathology, Instituto Nacional de Ciencias Médicas y Nutrición "Salvador Zubirán," 14080 Mexico City, Mexico

Contributed by Richard N. Zare, March 13, 2019 (sent for review July 19, 2018; reviewed by Gaurav Chopra and Lei Fu)

Two 1,4-benzoquinone derivatives, found in the venom of the scorpion *Diplocentrus melici* following exposure to air, have been isolated, characterized, synthesized, and assessed for antimicrobial activities. Initially a white, viscous liquid, the extracted venom colors within minutes under ambient conditions. From this colored mixture, two compounds, one red, the other blue, were isolated and purified using chromatography. After a variety of NMR and mass spectrometry experiments, the red compound was determined to be 3,5- dimethoxy-2-(methylthio)cyclohexa-2,5-diene-1,4-dione, and the blue compound was determined to be 5-methoxy-2,3- bis(methylthio) cyclohexa-2,5-diene-1,4-dione. Because extremely small amounts of these compounds were isolated from the scorpion venom, we developed laboratory syntheses from commercially available precursors, allowing us to produce sufficient quantities for crystallization and biological assays. The red benzoquinone is effective against *Staphylococcus aureus* [minimum inhibitory concentration (MIC) = 4 μg/mL], while the blue benzoquinone is active against *Mycobacterium tuberculosis* (MIC = 4 μg/mL) and even against a multidrug-resistant (MDR) strain with nearly equal effectiveness. The bactericidal effects of both benzoquinones show comparable activity to commercially available antibiotics used against these pathogens and were cytotoxic to neoplastic cell lines, suggesting their potential as lead compounds for the development of novel antimicrobial and anticancer drugs. Importantly, the blue benzoquinone was also effective in vivo with mouse models of MDR tuberculosis infection. After treatment for 2 mo, four mice with late-stage active MDR tuberculosis had a significant decrease in pulmonary bacillary loads and tissue damage. Healthy mice served as negative controls and tolerated treatment well, without adverse side effects.

mycobacterium tuberculosis | scorpion venom | antimicrobial activity | benzoquinones | *Staphylococcus aureus*

Worldwide, scorpion stings are a significant source of morbidity and mortality, annually disabling ∼1.5 million humans (1, 2). Initial investigations into scorpion venom were focused on isolating and structurally characterizing poisonous compounds. Such studies inspired the development of effective antivenom therapies, mainly antibodies generated in hyperimmunized horses (3). The first biochemical studies revealed that the majority of these toxin compounds are peptides that interfere with Na^+, K^+, Ca^{2+}, and Cl^- ion channels in target tissues (4–8). Not all compounds in scorpion venom are injurious to human health. Indeed, in recent years, compounds with a variety of beneficial properties, including antibacterial (9), antimalarial (10), and antiinflammatory activity (11), have been isolated (12). Most venom components described thus far are small peptides and large proteins. Isolation of nonproteinic components is an area of emerging research (13).

Globally, there are over 2,300 different scorpion species; of these, the venom of only ∼1% has been characterized (14). Within just Mexico, there are at least 281 different species of scorpions. Scorpions of the *Centruroides* genus, Buthidae family, are dangerous to humans and have been well studied (14). Among the 20 different known families of scorpions, there are some, including the Diplocentridae family, for which there exists no analysis of the venom (14). We describe here the isolation, structural characterization, synthesis, and biological activity of colored benzoquinone compounds derived from the venom of the scorpion *Diplocentrus melici* (Diplocentridae family). Their structures have been elucidated using a combination of mass spectrometry and NMR experiments. Chemical synthesis of these compounds yielded sufficient quantities for crystallization and structural confirmation by X-ray diffraction. Biological assays revealed that the red compound is very effective at killing *Staphylococcus aureus* and that the blue compound has remarkable activity against *Mycobacterium tuberculosis*. Of special

Significance

Development of new drugs from the venom of dangerous animals (spiders, snakes, scorpions, snails) has recently attracted much chemotherapeutic interest. While most isolated and characterized venom components are found to be proteinic or peptidic in nature, here we report two 1,4-benzoquinone compounds, one red and another blue, derived from the venom of a rarely studied scorpion (*Diplocentrus melici*) indigenous to Mexico. After successful identification and synthesis of these compounds, the red and blue benzoquinones showed remarkable antimicrobial activities against *Staphylococcus aureus* and *Mycobacterium tuberculosis*, respectively. The observation that the blue compound is equally effective against normal and multidrug-resistant tuberculosis while appearing not to affect the epithelium of lungs heightens its potential as a new drug candidate.

Author contributions: R.H.-P., L.D.P., and R.N.Z. designed research; E.N.C.-N., S.S., S.B., E.G., M.M.-T., D.M.-E., R.H.-P., J.I.V.-B., and L.D.P. performed research; E.N.C.-N., S.S., S.B., E.G., M.M.-T., D.M.-E., R.H.-P., J.I.V.-B., L.D.P., and R.N.Z. analyzed data; and E.N.C.-N., S.S., S.B., R.H.-P., L.D.P., and R.N.Z. wrote the paper.

Reviewers: G.C., Purdue University; and L.F., Shanghai Jiao Tong University.

The authors declare no conflict of interest.

[1]E.N.C.-N., S.S., and S.B. contributed equally to this work.

[2]To whom correspondence may be addressed. Email: possani@ibt.unam.mx or zare@stanford.edu.

This article contains supporting information online at www.pnas.org/lookup/suppl/doi:10.1073/pnas.1812334116/-/DCSupplemental.

Published online June 10, 2019.

importance is the finding that the blue compound is nearly as effective against multidrug-resistant tuberculosis (MDR-TB). Additionally, both compounds were found to be cytotoxic to human neoplastic cell lines and to mononuclear cells [peripheral blood mononuclear cells (PBMCs)].

Results

Isolation and Purification of the Red and Blue Compounds from the Venom. The total venom extracted by electrical stimulation from the telson of *D. melici* was first exposed to air until its color changed from white to dark red (*SI Appendix*, Fig. S1). This red-colored, viscous liquid was dissolved in ammonium acetate (20 mM, pH 4.7) and separated by gel filtration in a Sephadex G-50 column into three major fractions (labeled FI, FII, FIII in *SI Appendix*, Fig. S2*A*). FI was colorless and had a strong absorption at 280 nm, suggesting a composition largely of peptides, as shown by previous studies on scorpion venom (8). In contrast, fractions FII and FIII were red and had strong absorbances at both 280 and 325 nm. Interestingly, when lyophilized, fractions FII and FIII yielded a red and blue powder, respectively. FII and FIII were further purified by reversed-phase chromatography (HPLC) (C18 column, 0 to 60% acetonitrile in water, 60 min) as shown in *SI Appendix*, Fig. S2*B*. An intense peak at 25.2 min in the chromatogram corresponded to a single red compound (red in solution and in dried state), and another at 32.7 min corresponded to a single blue compound (red in solution but blue in dried state), which were then collected and dried for structural characterization and evaluation of biological activities. We suspected that these colored compounds were formed by oxidation of native compounds present in the *D. melici* venom. This transformation started within the first seconds of exposure to air (*SI Appendix*, Fig. S1*A*). Within 10 min, the entire liquid reddened (*SI Appendix*, Fig. S1*B*). To isolate the precursors of these colored compounds, we performed an alternative purification protocol. We found, serendipitously, that the rate of oxidation of the red and blue compounds is markedly reduced when the venom is dissolved in acetone. Rapid fractionation of this acetonic solution by HPLC yielded six main peaks (*SI Appendix*, Fig. S3*A*). Peaks 4 and 6 can be attributed to the red and the blue compounds, respectively. The fractions corresponding to the peaks were recovered and bubbled with air to promote oxidation with dissolved oxygen. After treatment, the compound in peak 2 underwent a shift in the retention time from 13.06 min to 25.05 min (*SI Appendix*, Fig. S4*A*). Similarly, the compound in peak 5 underwent a shift in retention time from 28.09 min to 32.63 min (*SI Appendix*, Fig. S4*B*). After prolonged exposure to air, the compounds in these fractions had the same ultraviolet-visible absorbance spectra as the red and blue compounds. It is thus likely that the compounds contained in peaks 4 and 6 before oxidation are precursors of the red and blue compounds. Fractions corresponding to peaks 1 and 3 did not change color upon exposure to air; at present, the composition of these peaks remains unknown. The precursor components 2 and 5 were assayed for possible inhibitory effect on *S. aureus* using a disk diffusion assay. No inhibition was observed, as shown in *SI Appendix*, Fig. S3*B*. There was no appearance of color on the disks or in the agar during the incubation time.

Structural Characterization of the Red and Blue Compounds. The red and blue compounds were electrosprayed from a methanolic solution, which produced ion signals of both protonated and metallated species (*SI Appendix*, Figs. S5 and S6). Both high mass accuracy and isotope distribution data suggested the molecular formulas $C_9H_{10}O_4S$ and $C_9H_{10}O_3S_2$ for the red and blue compounds, respectively, indicating, in each case, five degrees of unsaturation (number of rings and double bonds), calculated as one-half the sum of (twice the number of carbon atoms plus 2 minus the number of hydrogen atoms). The experimental mass-to-charge (m/z) accuracy was 0.28 parts per million (ppm) for the red compound and 0.43 ppm for the blue compound (*SI Appendix*, Figs. S5 and S6). Hydrogen–deuterium exchange experiments with each compound did not show evidence indicating the presence of exchangeable hydrogens (−OH, −SH, etc.) in each molecule. The tandem mass spectrometric study (*SI Appendix*, Figs. S7 and S8) using collision-induced dissociation on the protonated species (m/z 215.0365) for the red compound and the protonated species (m/z 231.0145) for the blue compound indicated the presence of carbonyl (C=O), methylthio (−SMe), and methoxy (−OMe) functional groups in the structure of each compound. The ^{1}H NMR (*SI Appendix*, Fig. S9) spectrum strongly suggested the presence of one −SMe functional group (δH 2.55, s, 3H) and two −OMe functional groups [(δH 3.81, s, 3H) and (δH 3.95, s, 3H)] in the red compound. For the blue compound, the same experiment (*SI Appendix*, Fig. S10) strongly suggests the presence of two −SMe functional groups [(δH 2.64, s, 3H) and (δH 2.52, s, 3H)] and one −OMe functional group (δH 3.81, s, 3H). A singlet signal of one proton at δH 5.96 for the red compound and δH 6.01 for the blue compound was also detected, possibly suggesting the presence of a vinylic proton in each molecule. We did not observe ^{1}H–^{1}H COSY correlation in each molecule, suggesting the lack of spin–spin coupling between neighboring protons. We could not record the ^{13}C NMR with the amount of wild-type compound (~0.5 mg) we extracted. However, we recorded the individual carbon chemical shifts from heteronuclear multiple-bond correlation (HMBC) and heteronuclear single quantum coherence experiments (vide infra). Because of low sample amounts, the HMBC experiment was conducted in a Shigemi advanced NMR tube (solvent: methanol-d4), and the results are shown in *SI Appendix*, Figs. S11 and S12. Detailed analysis of carbon–hydrogen correlation in HMBC revealed that the red and blue compounds are quinone derivatives, 3,5-dimethoxy-2-(methylthio)cyclohexa-2,5-diene-1,4- dione and 5-methoxy-2,3-bis(methylthio)cyclohexa-2,5-diene-1,4-dione, respectively, whose structures are given in Fig. 1. *SI Appendix*, Figs. S11 and S12 list the individual chemical shifts of protons and carbons. The nuclear Overhauser effect study also revealed the proximity of a vinylic proton (δH 5.96) to the −OMe functional group (δH 3.81) in the

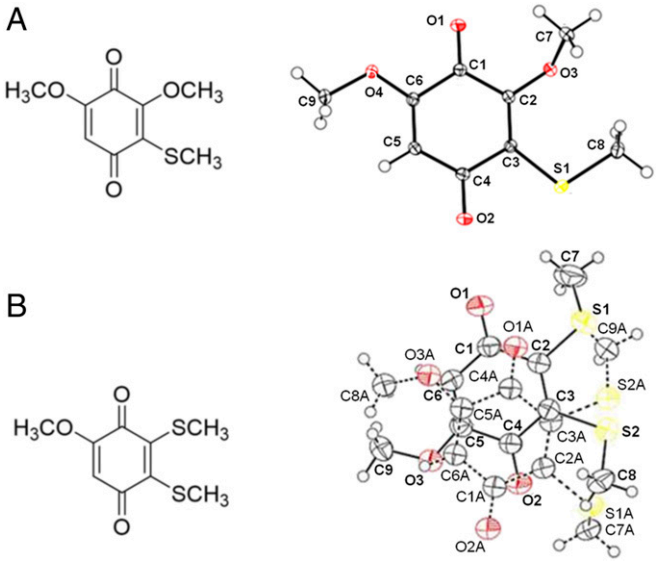

Fig. 1. (*Left*) Structures of (*A*) red and (*B*) blue compounds extracted from the venom of *D. melici*. (*Right*) Corresponding X-ray crystallographic data (Cambridge Crystallographic Data Center No. 0001001197099) of the synthetic molecules (oxygen and sulfur atoms are presented in red and yellow, respectively) (see *SI Appendix* for details).

red compound and the proximity of a vinylic proton (δH 6.01) to the −OMe functional group (δH 3.81) in the blue compound. As the structures of the red and blue compounds have been established as 1,4-benzoquinones, the molecules corresponding to peaks 2 and 5 (*SI Appendix*, Fig. S3) are likely to be precursor hydroquinones, which were oxidized in air to form 1,4-benzoquinones as discussed before (*SI Appendix*, Fig. S13). Finally, we synthesized each benzoquinone derivative (see below), and the structure of each synthesized compound was further verified by comparing its NMR data with wild-type compounds; see *SI Appendix*, Fig. S14 and associated material in *SI Appendix*.

Chemical Synthesis of the Red and Blue Benzoquinones. We synthesized the red compound in a two-step procedure as shown in *SI Appendix*, Scheme S1 (see *SI Appendix* for details of the synthesis). Commercially available 3,4,5-trimethoxyphenol **1** was reacted with dimethyl disulfide in the presence of aluminum chloride in a Friedel–Crafts-type reaction to form 3,4,5-trimethoxy-2-(methylthio)phenol **2** with moderate yield of 24%. This intermediate was oxidized with ceric ammonium nitrate (CAN) and recrystallized from 1:4 EtOAc/hexanes to yield (35%) red crystals of the desired benzoquinone compound **3** (X-ray crystal structure shown in Fig. 1).

SI Appendix, Scheme S2 illustrates the synthesis of the blue compound (see *SI Appendix* for details of synthesis). Commercially available 1,4-dimethoxy-2,3-dibromobenzene **4** was oxidized with CAN to provide 2,3-dibromo-1,4-benzoquinone **5** in an almost quantitative reaction. A Diels–Alder cycloaddition between **5** and excess, freshly distilled cyclopentadiene proceeded smoothly at room temperature, yielding tricyclic compound **6**. Using the optimized protocol of Ferreira et al. (15), the bromides were replaced with thiomethoxy groups in a fast reaction conducted in a separatory funnel. Heating **7** with an excess of $NaHCO_3$ in a 1:1:1 mixture of tetrahydrofuran/MeOH/H_2O gave the enol tautomer **8**. Treatment of **8** with $Fe_2(SO_4)_3$ in acidic MeOH at 60 °C for 12 h led to rapid oxidation to the 1,4-benzoquinone; compounds **9** and **9′** formed via a 1,4-addition of MeOH to this benzoquinone. A *retro*-Diels–Alder reaction was effected at 120 °C to yield the blue benzoquinone **10** (X-ray crystal structure shown in Fig. 1).

Biological Activity of the Red and Blue Benzoquinones. We evaluated the inhibitory activity of the red and blue benzoquinones against *S. aureus* using a disk diffusion assay. There is a clear inhibition of *S. aureus* growth by the action of the red and blue benzoquinones (Fig. 2*A*). Based on the diameters of inhibition, the red benzoquinone is more active than the blue benzoquinone. We confirmed this difference using a broth microdilution assay (Fig. 2*B*). The minimum inhibitory concentration (MIC) for *S. aureus* growth is 4 μg/mL for the red benzoquinone and 6 μg/mL for the blue benzoquinone (Fig. 2*B*). Ampicillin (MIC = 0.5 μg/mL) was used as a positive control (16, 17). These compounds are bactericidal at their MICs, killing 90% of *S. aureus* in 6 h and 99.9% in 24 h (*SI Appendix*, Table S1). Neither benzoquinone showed activity against *Escherichia coli* (Gram$^-$ bacteria) and *Candida albicans* (pathogenic fungus).

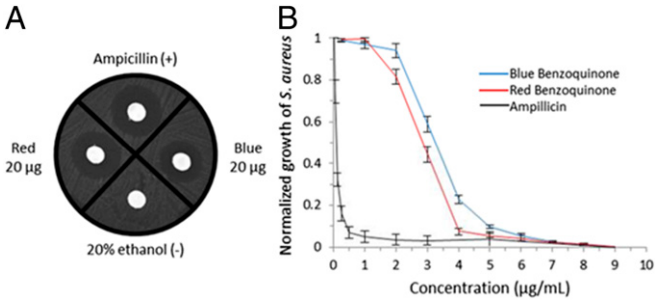

Fig. 2. Inhibition of *S. aureus*. (*A*) Disk diffusion assay of red and blue benzoquinones showing activity against *S. aureus*. Ampicillin (5 μg) was used as a positive control. (*B*) Determination of the MICs of the red and blue benzoquinones against *S. aureus*. The MICs determined by the broth microdilution assay are 4 μg/mL for the red benzoquinone and 6 μg/mL for the blue benzoquinone. Ampicillin was used as a positive control. Each result is reported as the mean ± SD.

Likewise, using a broth microdilution assay, we tested the efficacy of both benzoquinones in killing *M. tuberculosis* H37Rv [a pathogenic strain commonly used in such studies (18)] and an MDR strain from clinical isolates. Interestingly, only the blue benzoquinone showed significant inhibitory activity against *M. tuberculosis* (H37Rv and MDR) with an MIC of 4 μg/mL for both strains (Fig. 3*A*), which is similar to the MICs reported for isoniazid, rifampicin, ethambutol, levofloxacin, moxifloxacin, and capreomycin against sensitive strains of *M. tuberculosis* (19–21). The red benzoquinone was inhibitory only at concentrations higher than 160 μg/mL, which was assumed to be inappropriate for antibiotic development (22). In an independent test of efficacy, the concentration of colony-forming units (CFUs) of bacteria growing after treatment was determined. There was a clear reduction in the concentration of CFUs after treatment with the benzoquinones at doses equivalent to their MICs (Fig. 3*B*), especially by the blue benzoquinone in the MDR strain with more than 90% of killing in comparison with the inoculum bacteria concentration. Additionally, ultrastructural changes were promoted by the action of the blue benzoquinone in the *M. tuberculosis* bacilli (Fig. 3 *C*–*F*). These were similar to what occurs when the bacteria are exposed to isoniazid (Fig. 3 *G* and *H*), an effective antimycobacterial antibiotic that interferes with cell wall synthesis. There is a clear loss of the elongated bacillus cytomorphology as well as the formation of cytoplasmic electrodense conglomerates with extensive cell wall effacement.

The bactericidal activity of the blue compound was tested against progressive pulmonary TB using an experimental infection model in BALB/c mice. Eight micrograms of the blue benzoquinone was administered by an intratracheal route every other day for 2 mo; during this time, infected mice showed a clear improvement by not losing weight and not showing piloerection (which are usual signs in mice affected with progressive pulmonary TB). They also showed a significant reduction of the lung bacillary load (greater than 90%) in comparison with the negative control (infected mice simply treated with saline solution) (Fig. 4*A*). This result correlated well with the histological changes; treated mice showed a twofold decrease of tissue damage (pneumonia) compared with control animals (Fig. 4*B*). Importantly, this same dose was administered intratracheally to healthy mice for 1 mo, after which they were killed and their lungs examined. Their pulmonary histology was almost completely normal, with only minor inflammatory infiltrates found around the venules. We could not appreciate any fibrosis.

Because of the potential of these benzoquinones to serve as lead compounds for new antibiotics, we were interested in evaluating their toxicity to human cell lines. We began by evaluating the viability of a lung adenocarcinoma cell line, A549, which has served as a model of alveolar Type II pulmonary epithelium (23, 24). In the presence of the red and blue benzoquinones at concentrations of 1, 5, and 25 μM, the A549 cells remained relatively unaffected (*SI Appendix*, Fig. S15), suggesting that the direct application of these benzoquinones to lungs for the treatment of TB may be possible. Under the same in vitro conditions, we found that, after a 12-h culture period, the red and blue benzoquinones were comparably potent in inducing death of Jurkat (T-cell leukemia cell line), TE 671 (rhabdomyosarcoma cell line), and SH-SY5Y (bone marrow neuroblastoma cell line) (*SI Appendix*, Fig. S15). We also examined two types of cells commonly found in human blood, erythrocytes and PBMCs. Even at doses higher than 100 μg/mL, no erythrocyte

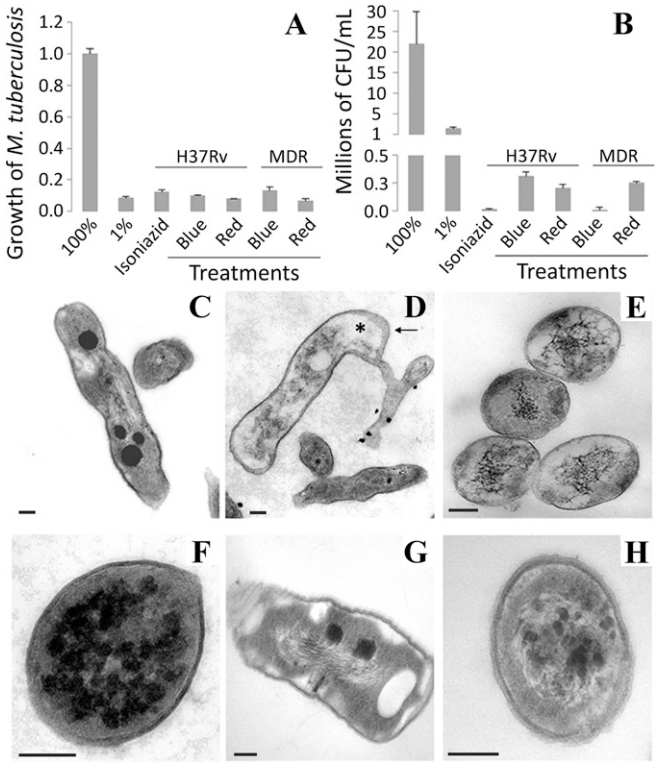

Fig. 3. Inhibitory activity (in vitro) of blue and red benzoquinones against *M. tuberculosis* (H37Rv and MDR strain). (*A*) MICs were determined by broth microdilution, and bacterial proliferation was evaluated by a colorimetric assay using Cell Titer 96 Aqueous. For both strains, the MIC of the blue benzoquinone against *M. tuberculosis* is 4 μg/mL. The red benzoquinone had an MIC of 160 μg/mL, which is considered unsuitable for clinical use. (*B*) Viability of the bacteria was evaluated by counting the CFUs resulting after treatment at the MIC. Each result is reported as the mean ± SD. (*C*–*F*) Ultrastructural changes in *M. tuberculosis* in response to the blue benzoquinone. To examine the cytotoxic effect of benzoquinone against *M. tuberculosis*, the ultrastructure of bacilli after treatment with the blue benzoquinone was examined. (*C*) Control untreated bacilli showed a well-defined, homogeneous and slightly electron-lucent cell wall, while the cytoplasm was generally electron-lucent with some lipid medium-sized vacuoles. (*D*) Incubation with benzoquinone produced substantial abnormalities, such as extensive effacement of cell wall (arrow) and cytoplasmic extraction (asterisk). (*E* and *F*) Conglomerates of electron dense reticular filaments located in the central areas of the cytoplasm. (*G* and *H*) Similar subcellular changes were induced by isoniazid incubation. (Scale bars: 100 nm.)

hemolysis was observed after 2 h (*SI Appendix*, Fig. S16*A*). However, at a concentration of 25 μM, the blue and red benzoquinones killed 50% and 60% of PBMCs, respectively, after 12 h (*SI Appendix*, Fig. S16*B*).

We performed an in vitro glutathione oxidation assay as a first step in investigating the mechanism underlying the marked cytotoxicity of these 1,4-benzoquinone compounds. Both benzoquinones oxidized glutathione to the corresponding derivatives in a dose-dependent manner (*SI Appendix*, Fig. S17); this suggests that depletion of glutathione, an important cellular antioxidant, may play a role in triggering cell death (25). In preliminary studies (*SI Appendix*, Fig. S18), we found that incubation of cells with the benzoquinones leads to the formation of reactive oxygen species (ROS) and a time-dependent loss of the cell membrane asymmetry, suggesting an apoptotic mode of cell death.

Discussion

Compounds with the 1,4-benzoquinone motif are a large class of molecules distributed throughout nature. They are highly reactive, acting as both oxidants and Michael acceptors, and many have been serendipitously found to have antimicrobial, antineoplastic, anticoagulant, and analgesic activity (26–32). In this work, we describe two 1,4-benzoquinone compounds, one red, the other blue, which are derived from naturally occurring precursors in the venom of *D. melici*, a scarcely studied species of scorpion which is indigenous to Mexico. The naturally occurring precursors rapidly oxidize upon exposure to air; while their identities could not be conclusively determined, it is highly likely that they are the corresponding hydroquinones (*SI Appendix*, Fig. S13) (33). It is currently unknown why the scorpion telson contains such oxidatively labile compounds in great abundance.

To gain access to sufficient quantities of both benzoquinones for biological testing, we designed synthetic routes from commercially available reagents. The resulting synthetic benzoquinones have the same structure, biological activity, and physicochemical properties. Through empiric screening, we found, fortuitously, that these colored benzoquinones have great potential as lead compounds for the development of antimicrobial agents against *S. aureus* and *M. tuberculosis*. Against *S. aureus*, both compounds are highly active, with potencies comparable to commercially used antibiotics (16); the red benzoquinone is slightly more active than the blue one (MIC of 4 μg/mL vs. MIC of 6 μg/mL). It should be noted that the inhibitory activity of both compounds is superior to that of other naturally occurring benzoquinones known to inhibit the growth of *S. aureus* (34, 35). Despite such dramatic activity against *S. aureus* ($Gram^+$ bacteria), neither compound was found to have appreciable activity against *E. coli* ($Gram^-$ bacteria). Previous studies have delineated that substitution at the 3rd position of 2,6-dimethoxybenzoquinone dramatically decreases its activity against *E. coli* (30). By analogy, it is possible that the thiomethoxy group is responsible for the selectivity seen in our compounds.

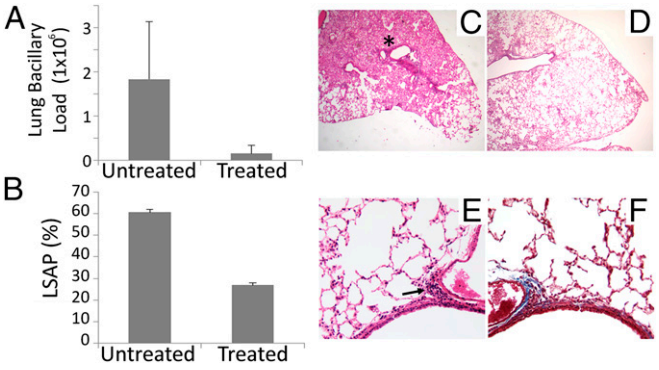

Fig. 4. Inhibitory activity (in vivo) of the blue benzoquinone against *M. tuberculosis*. For this, we used an experimental model of progressive pulmonary tuberculosis consisting of BALB/c mice infected with the MDR CIBIN99 strain. Mice were treated for 2 mo with the blue benzoquinone using a dose of 8 μg administered by intratracheal route every other day. After the 2 mo, the group of mice treated with the blue benzoquinone had a marked improvement in their condition, with (*A*) a reduction of more than 90% of the lung bacillary load (evaluated by counting the CFUs) compared with the untreated group. (*B*) A clear reduction in the percentage of lung surface affected by pneumonia (LSAP) was observed in the lungs of the treated group. This difference is confirmed by automated histomorphometry, which shows a 50% reduction of pneumonia posttreatment. (*C*) Representative micrograph of a lung (hematoxylin-eosin staining) from the untreated group showing extensive areas of pneumonia (asterisk). (*D*) There is less pneumonia in lungs of the treated group. (*E*) Representative micrograph of a healthy mouse treated intratracheally for 1 mo with 8 μg of the blue benzoquinone. The pulmonary histology is normal, with the exception of occasional mild inflammatory infiltrates found around venules (arrow). (*F*) There is no fibrosis in the lungs of these healthy control mice (trichrome Masson staining). (Magnification: *C* and *D*, 25×; *E* and *F*, 200×.)

In addition to the antimicrobial activity against *S. aureus*, both benzoquinones inhibit the growth of *M. tuberculosis*, with the blue benzoquinone being more promising for a clinical application (MIC of 4 μg/mL) (Fig. 3). There is a reduction in the bacterial concentration after the treatment for both benzoquinones in comparison with the initial inoculum concentration of *Mycobacteria* (2.5×10^6 bacteria per milliliter), suggesting bactericidal activity. Interestingly, this in vitro bactericidal effect is higher in the MDR strain, with the blue benzoquinone killing more than 90% of the bacteria load at the MIC (Fig. 3*B*). More importantly, this bactericidal effect is conserved in an in vivo experimental infection mouse model; treated mice have a marked diminution of the bacillary load and a clear decrease in tissue damage. The MIC of the blue benzoquinone (4 μg/mL) is markedly lower than related compounds that appear in the literature, including lapachol (MIC = 100 μg/mL), 1,4-napthoquinone (MIC = 100 μg/mL), and 1,4-benzoquinone (MIC = 25 μg/mL) (36).

The high ROS production produced by benzoquinones in eukaryotic cells could be also the mechanism of the antimycobacterial activity. Several bactericidal antibiotics with a variety of different mechanisms of action increase ROS production within cells via the Fenton reaction (37, 38). Numerous ROS, in particular, hydroxyl radicals, induce bacterial death via DNA damage, which is caused, in part, by the oxidation of the guanine nucleotide pool (39). The remarkable activity against the MDR strain proves the potential of the blue benzoquinone as a lead molecule for treatment of infection caused by MDR *M. tuberculosis*.

It is also worth commenting on the cytotoxicity of these compounds to T-cell leukemia, rhabdomyosarcoma, and metastatic neuroblastoma but not in the lung adenocarcinoma cell line (*SI Appendix*, Fig. S15), suggesting a selectivity for some cell lines. The 1,4-benzoquinone compounds are oxidatively very labile; they are easily reduced to semiquinones which are rapidly reoxidized by molecular oxygen. This vigorous redox activity generates a multitude of ROS as byproducts, including peroxides, superoxides, and hydroxyl radicals (40, 41). By oxidizing thiol groups into disulfides, these ROS deplete intracellular glutathione and cause protein aggregation and malfunction (42, 43). ROS irreversibly damage other biological macromolecules essential to cell survival, including lipids and nucleic acids (44, 45). Once cellular damage reaches a threshold, apoptotic pathways are initiated for systematic cell death. Such is the mechanism of action of the naturally occurring cytotoxic quinones doxorubicin, daunorubicin, and mitomycin C, which are clinically used chemotherapeutic agents (40).

In this matter, the apoptotic activity mediated by ROS could enhance the antimicrobial activity against intracellular *M. tuberculosis*, because it is known that this pathogen inhibits apoptosis of infected macrophages (46, 47). Induction of apoptosis plus the direct bactericidal activity of the blue benzoquinone could have a synergistic effect in the eradication of TB in vivo. Further studies are required to determine whether these red and blue benzoquinones can serve as new antibiotics.

Materials and Methods

SI Appendix, Materials and Methods provides details of the purification and structural characterization of venom components (red and blue) along with their syntheses.

***S. aureus* Inhibition Assays.** Red and blue benzoquinones were tested against *S. aureus* by disk diffusion and broth microdilution assays. First, the red-colored benzoquinones were solubilized in 20% ethanol, and the concentration was determined using experimental coefficients at 325 nm [Red, $\varepsilon = 0.02524$ (mL μg^{-1} cm^{-1}) and Blue, $\varepsilon = 0.0407$ (mL μg^{-1} cm^{-1})]. For the disk diffusion assay, 150 μL of mid-log–phase culture (Absorbance = 0.5 at 600 nm) of *S. aureus* were evenly spread on a Mueller Hinton agar plate. The plate was allowed to dry to eliminate excess liquid. Once the agar was dry, filter disks loaded with 20 μg of each colored component were placed in the plate. A disk with 10 μg of ampicillin was used as a positive control and a disk with 20% ethanol served as a negative control of growth inhibition. The plate was incubated at 37 °C for 12 h. Subsequently, a broth microdilution assay was performed to determinate the MIC. A range of concentrations (0 mg/mL to 9 μg/mL) was evaluated. The assay was performed using a final volume of 200 μL per sample in a 96-well plate. Culture growth was initiated in Mueller Hinton broth using an inoculum of *S. aureus* equivalent to a 1:200 dilution of a 0.5 McFarland standard. Bacterial culture was incubated at 37 °C with orbital shaking at 150 rpm for 24 h. After incubation, culture growth was evaluated by the absorbance at 600 nm. The MICs were determined by the concentration at which no growth was observed. Bactericidal effect was determined for both benzoquinones by time-kill assay at the MIC as described by Konate et al. (48).

***M. tuberculosis* Inhibition Assay.** For this assay, the red and blue benzoquinones were tested by broth microdilution inhibition assay using the virulent strain of *M. tuberculosis* H37Rv and an MDR strain CIBIN99, which is a clinical isolate resistant to all of the primary antibiotics. Assay was performed in 96-well plates as described previously (49). An initial load of 3×10^5 bacteria was inoculated per well in Middlebrook 7H9 broth (Difco Laboratories) at final volume of 200 μL. A range of 0.125 mg/mL to 16 μg/mL of the benzoquinones was initially tested. Cultures were incubated for 7 d at 35 °C. Bacteria proliferation was determined by a colorimetric assay using Cell Titer 96 Aqueous and measuring the absorbance at 492 nm.

Transmission electron microscopy. Additionally, the ultrastructural damage to *M. tuberculosis* caused by the benzoquinone treatment was evaluated using transmission electron microscopy. Briefly, bacilli were cultured in Middlebrook 7H9 broth supplemented with Middlebrook OADC (oleic albumin dextrose catalase) enrichment media (BBL; BD) until logarithmic phase was achieved. Viable bacilli (1×10^7) were placed in the wells of 96-well plates and were exposed to the benzoquinone compound for 18 h at the MICs determined previously. Subsequently, fixation was performed by immersion in 4% glutaraldehyde in cacodylate buffer for 4 h, followed by exposition to fumes of osmium tetraoxide. As a control, the same conditions were used to prepare bacteria incubated with isoniazid. The bacterial suspension was then centrifuged to form a pellet that was later dehydrated with graded ethyl alcohol solutions and embedded in Epon resin (London Resin Company). Thin sections of 70 nm to 90 nm width were placed on copper grids and were contrasted with uranium salts and lead citrate (Electron Microscopy Sciences), and were examined with a Technai FEI electron microscope.

Experimental Model of Progressive Pulmonary TB. The MDR strain CIBIN99 was grown in Middlebrook 7H9 broth supplemented with Middlebrook OADC enrichment media and 0.02% Tween 80 at 37 °C. Mid-log–phase culture was used for all experiments. The experimental model of progressive pulmonary TB has been described in detail elsewhere (49, 50). Briefly, male BALB/c mice aged 6 wk to 8 wk were anesthetized in a gas chamber using 0.1 mL per mouse of sevoflurane, and each mouse was infected by endotracheal instillation with 2.5×10^5 live bacilli. Mice were maintained in the vertical position until they underwent spontaneous recovery. Infected mice were maintained in groups of five in cages fitted with microisolators. All procedures were performed in a biological security cabinet at a Biosafety level III facility. Animal work was performed in accordance with Mexican national regulations on Animal Care and Experimentation (NOM 062-ZOO-1999) and according to the guidelines and approval of the Ethical Committee for Experimentation in Animals of the National Institute of Medical Sciences and Nutrition in Mexico City, permit number CINVA 1825 PAT-1825-16/18-1.

After 60 d of infection, animals were arbitrarily divided into treated and control groups. The treated group was tested with a dose of 8 μg of the blue compound dissolved in 50 μL of saline solution and administered by intratracheal route every other day for 2 mo, while the control group received only the vehicle solution. The selection of the appropriate dose was calculated according to the MIC determined in vitro (drug concentration needed to kill 1×10^6 bacilli) by adjusting the drug concentration to the estimated number of bacilli in the lungs of the mice after 2 mo of infection. The efficiency of the treatment was determined by quantifying the lung bacillary loads by assessing CFUs and the extent of tissue damage by histopathology and automated morphometry.

For the determination of bacillary loads and histopathology, immediately after the animals were killed by exsanguination under anesthesia with intraperitoneal pentobarbital, the lungs were removed; the right lung was immediately frozen by immersion in liquid nitrogen and used for CFU determination, while the left lung was perfused for histopathology analysis. For CFU determination, frozen lungs were disrupted using ceramic beads in tubes with 1 mL of phosphate-buffered saline containing 0.05% tween. Four

dilutions of each homogenate were spread onto duplicate plates containing Bacto Middlebrook7H10 agar enriched with OADC. The incubation time of the plates was 21 d, and data points are the means of three animals. For the determination of tissue damage (pneumonia) by histomorphometry, the left lung was perfused via trachea with 100% ethanol and immersed for 24 h in the same fixative. Parasagittal sections were taken through the hilum, and these were dehydrated and embedded in paraffin, and histological sections stained with hematoxylin and eosin were obtained. The percentage of lung area affected by pneumonia was measured using a Leica Q-win Image Analysis System. Measurements were performed in a blind manner, and data are expressed as the mean of three animals ±SD.

ACKNOWLEDGMENTS. We acknowledge the support and help received from Diego Martínez Otero for the X-ray diffraction study, Stephen R. Lynch for the NMR study, and J. C. Leon-Contreras for the ultrastructural study. S.B. thanks Science and Engineering Research Board, Department of Science and Technology, India, for providing a Ramanujan Fellowship Research Grant. This work was supported by the Air Force Office of Scientific Research through Basic Research Initiative Grant AFOSR FA9550-16-1-0113.

1. Epidemiología DGd, "Manual de Procedimientos Estandarizados para la Vigilancia Epidemiológica de la Intoxicación por Picadura de Alacrán" (Secretaría de Salud, Salud SdPyPdl, 2012).
2. J. P. Chippaux, Emerging options for the management of scorpion stings. *Drug Des. Devel. Ther.* **6**, 165–173 (2012).
3. G. P. Espino-Solis, L. Riaño-Umbarila, B. Becerril, L. D. Possani, Antidotes against venomous animals: State of the art and prospectives. *J. Proteomics* **72**, 183–199 (2009).
4. M. D. Cahalan, Modification of sodium channel gating in frog myelinated nerve fibres by *Centruroides sculpturatus* scorpion venom. *J. Physiol.* **244**, 511–534 (1975).
5. W. A. Catterall, Cooperative activation of action potential Na+ ionophore by neurotoxins. *Proc. Natl. Acad. Sci. U.S.A.* **72**, 1782–1786 (1975).
6. H. Rochat, P. Bernard, F. Couraud, Scorpion toxins: Chemistry and mode of action. *Adv. Cytopharmacol.* **3**, 325–334 (1979).
7. F. Miranda, C. Kupeyan, H. Rochat, C. Rochat, S. Lissitzky, Purification of animal neurotoxins. Isolation and characterization of eleven neurotoxins from the venoms of the scorpions *Androctonus australis hector*, *Buthus occitanus tunetanus* and *Leiurus quinquestriatus quinquestriatus*. *Eur. J. Biochem.* **16**, 514–523 (1970).
8. L. D. Possani, E. Merino, M. Corona, F. Bolivar, B. Becerril, Peptides and genes coding for scorpion toxins that affect ion-channels. *Biochimie* **82**, 861–868 (2000).
9. A. Torres-Larios, G. B. Gurrola, F. Z. Zamudio, L. D. Possani, Hadrurin, a new antimicrobial peptide from the venom of the scorpion *Hadrurus aztecus*. *Eur. J. Biochem.* **267**, 5023–5031 (2000).
10. R. Conde, F. Z. Zamudio, M. H. Rodríguez, L. D. Possani, Scorpine, an anti-malaria and anti-bacterial agent purified from scorpion venom. *FEBS Lett.* **471**, 165–168 (2000).
11. G. B. Gurrola *et al*., Structure, function, and chemical synthesis of *Vaejovis mexicanus* peptide 24: A novel potent blocker of Kv1.3 potassium channels of human T lymphocytes. *Biochemistry* **51**, 4049–4061 (2012).
12. E. Ortiz, G. B. Gurrola, E. F. Schwartz, L. D. Possani, Scorpion venom components as potential candidates for drug development. *Toxicon* **93**, 125–135 (2015).
13. S. Banerjee *et al*., An alkaloid from scorpion venom: Chemical structure and synthesis. *J. Nat. Prod.* **81**, 1899–1904 (2018).
14. C. E. Santibáñez-López, O. F. Francke, C. Ureta, L. D. Possani, Scorpions from Mexico: From species diversity to venom complexity. *Toxins (Basel)* **8**, E2 (2015).
15. V. F. Ferreira, A. Park, F. J. Schmitz, F. A. Valeriote, Synthesis of perfragilin A, B and some analogues. *Tetrahedron* **59**, 1349–1357 (2003).
16. ESCMID Eo, Determination of minimum inhibitory concentrations (MICs) of antibacterial agents by broth dilution. *Clin. Microbiol. Infect.* **9**, ix–xv (2003).
17. R. Pieterse, S. D. Todorov, D. Leon M T, Mode of action and in vitro susceptibility of mastitis pathogens to macedocin ST91KM and preparation of a teat seal containing the bacteriocin. *Braz. J. Microbiol.* **41**, 133–145 (2010).
18. P. Bifani *et al*., Molecular characterization of *Mycobacterium tuberculosis* H37Rv/Ra variants: Distinguishing the mycobacterial laboratory strain. *J. Clin. Microbiol.* **38**, 3200–3204 (2000).
19. S. Chanwong, N. Maneekarn, L. Makonkawkeyoon, S. Makonkawkeyoon, Intracellular growth and drug susceptibility of *Mycobacterium tuberculosis* in macrophages. *Tuberculosis (Edinb.)* **87**, 130–133 (2007).
20. K. Kaniga *et al*., A multilaboratory, multicountry study to determine MIC quality control ranges for phenotypic drug susceptibility testing of selected first-line antituberculosis drugs, second-line injectables, fluoroquinolones, clofazimine, and linezolid. *J. Clin. Microbiol.* **54**, 2963–2968 (2016).
21. E. Sturegård *et al*., Little difference between minimum inhibitory concentrations of *Mycobacterium tuberculosis* wild-type organisms determined with BACTEC MGIT 960 and Middlebrook 7H10. *Clin. Microbiol. Infect.* **21**, 148.e5–148.e7 (2015).
22. J. M. Nguta, R. Appiah-Opong, A. K. Nyarko, D. Yeboah-Manu, P. G. Addo, Current perspectives in drug discovery against tuberculosis from natural products. *Int. J. Mycobacteriol.* **4**, 165–183 (2015).
23. K. A. Foster, C. G. Oster, M. M. Mayer, M. L. Avery, K. L. Audus, Characterization of the A549 cell line as a type II pulmonary epithelial cell model for drug metabolism. *Exp. Cell Res.* **243**, 359–366 (1998).
24. Y. Lin, M. Zhang, P. F. Barnes, Chemokine production by a human alveolar epithelial cell line in response to *Mycobacterium tuberculosis*. *Infect. Immun.* **66**, 1121–1126 (1998).
25. J. Butler, B. M. Hoey, Reactions of glutathione and glutathione radicals with benzoquinones. *Free Radic. Biol. Med.* **12**, 337–345 (1992).
26. K. T. Finley, "The addition and substitution chemistry of quinones" in *The Chemistry of Quinonoid Compounds (1974) Part 2* (Wiley, 1974) vol. 2, pp. 877–1144.
27. A. Brunmark, E. Cadenas, Reductive addition of glutathione to p-benzoquinone, 2-hydroxy-p-benzoquinone, and p-benzoquinone epoxides. Effect of the hydroxy- and glutathionyl substituents on p-benzohydroquinone autoxidation. *Chem. Biol. Interact.* **68**, 273–298 (1988).
28. I. Abraham, R. Joshi, P. Pardasani, R. T. Pardasani, Recent advances in 1,4-benzoquinone chemistry. *J. Braz. Chem. Soc.* **22**, 385–421 (2011).
29. J. S. Novais *et al*., Synthesis and antimicrobial evaluation of promising 7-arylamino-5,8-dioxo-5,8-dihydroisoquinoline-4-carboxylates and their halogenated amino compounds for treating Gram-negative bacterial infections. *RSC Adv.* **7**, 18311–18320 (2017).
30. E. J. Lana, F. Carazza, J. A. Takahashi, Antibacterial evaluation of 1,4-benzoquinone derivatives. *J. Agric. Food Chem.* **54**, 2053–2056 (2006).
31. D. Schulz *et al*., Abenquines A-D: Aminoquinone derivatives produced by streptomyces sp. strain DB634. *J. Antibiot. (Tokyo)* **64**, 763–768 (2011).
32. X. Zhang *et al*., Antibacterial meroterpenoids from the South China Sea sponge *Dysidea* sp. *Chem. Pharm. Bull. (Tokyo)* **64**, 1036–1042 (2016).
33. I. Hassan, J. Pavlov, R. Errabelli, A. B. Attygalle, Oxidative ionization under certain negative-ion mass spectrometric conditions. *J. Am. Soc. Mass Spectrom.* **28**, 270–277 (2017).
34. M. H. Kim *et al*., Antimicrobial activities of 1,4-benzoquinones and wheat germ extract. *J. Microbiol. Biotechnol.* **20**, 1204–1209 (2010).
35. A. Nishina, T. Uchibori, Antimicrobial activity of 2,6-dimethoxy-p-benzoquinone, isolated from thick-stemmed bamboo, its analogs. *Agric. Biol. Chem.* **55**, 2395–2398 (1991).
36. T. Tran *et al*., Quinones as antimycobacterial agents. *Bioorg. Med. Chem.* **12**, 4809–4813 (2004).
37. M. A. Kohanski, D. J. Dwyer, B. Hayete, C. A. Lawrence, J. J. Collins, A common mechanism of cellular death induced by bactericidal antibiotics. *Cell* **130**, 797–810 (2007).
38. X. Wang, X. Zhao, Contribution of oxidative damage to antimicrobial lethality. *Antimicrob. Agents Chemother.* **53**, 1395–1402 (2009).
39. J. J. Foti, B. Devadoss, J. A. Winkler, J. J. Collins, G. C. Walker, Oxidation of the guanine nucleotide pool underlies cell death by bactericidal antibiotics. *Science* **336**, 315–319 (2012).
40. M. Saibu, S. Sagar, I. Green, F. Ameer, M. Meyer, Evaluating the cytotoxic effects of novel quinone compounds. *Anticancer Res.* **34**, 4077–4086 (2014).
41. P. L. Gutierrez, The metabolism of quinone-containing alkylating agents: Free radical production and measurement. *Front. Biosci.* **5**, D629–D638 (2000).
42. C. Mytilineou, B. C. Kramer, J. A. Yabut, Glutathione depletion and oxidative stress. *Parkinsonism Relat. Disord.* **8**, 385–387 (2002).
43. D. Wilhelm, K. Bender, A. Knebel, P. Angel, The level of intracellular glutathione is a key regulator for the induction of stress-activated signal transduction pathways including Jun N-terminal protein kinases and p38 kinase by alkylating agents. *Mol. Cell. Biol.* **17**, 4792–4800 (1997).
44. X. Wang *et al*., Mechanism of arylating quinone toxicity involving Michael adduct formation and induction of endoplasmic reticulum stress. *Proc. Natl. Acad. Sci. U.S.A.* **103**, 3604–3609 (2006).
45. D. R. Green, J. C. Reed, Mitochondria and apoptosis. *Science* **281**, 1309–1312 (1998).
46. V. Briken, J. L. Miller, Living on the edge: Inhibition of host cell apoptosis by *Mycobacterium tuberculosis*. *Future Microbiol.* **3**, 415–422 (2008).
47. A. Lam *et al*., Role of apoptosis and autophagy in tuberculosis. *Am. J. Physiol. Lung Cell. Mol. Physiol.* **313**, L218–L229 (2017).
48. K. Konaté *et al*., Antibacterial activity against β- lactamase producing methicillin and ampicillin-resistants *Staphylococcus aureus*: Fractional inhibitory concentration index (FICI) determination. *Ann. Clin. Microbiol. Antimicrob.* **11**, 18 (2012).
49. A. Y. Coban, A. Birinci, B. Ekinci, B. Durupinar, Drug susceptibility testing of *Mycobacterium tuberculosis* by the broth microdilution method with 7H9 broth. *Mem. Inst. Oswaldo Cruz* **99**, 111–113 (2004).
50. R. Hernández-Pando *et al*., Correlation between the kinetics of Th1, Th2 cells and pathology in a murine model of experimental pulmonary tuberculosis. *Immunology* **89**, 26–33 (1996).